photonics

MDPI

Communication

High-Power Supersymmetric Semiconductor Laser with a Narrow Linewidth

Yuanbo Xu [1,2], Ting Fu [1,2], Jian Fan [1,2], Wenzhen Liu [1,2], Hongwei Qu [1,3], Mingjin Wang [1,3,*] and Wanhua Zheng [1,2,3,4,*]

[1] Laboratory of Solid State Optoelectronics Information Technology, Institute of Semiconductors, Chinese Academy of Sciences, Beijing 100083, China
[2] Center of Materials Science and Optoelectronics Engineering, University of Chinese Academy of Sciences, Beijing 100049, China
[3] State Key Laboratory on Integrated Optoelectronics, Institute of Semiconductors, Chinese Academy of Sciences, Beijing 100083, China
[4] College of Future Technology, University of Chinese Academy of Sciences, Beijing 101408, China
* Correspondence: mingjinwang@semi.ac.cn (M.W.); whzheng@semi.ac.cn (W.Z.)

Abstract: We have designed and fabricated a kind of supersymmetric slotted Fabry–Perot semiconductor laser near 1550 nm to achieve a single-mode, high-power, and narrow-linewidth operation. The structure of the laser is composed of an electrically pumped broad ridge waveguide in the middle to provide optical gain, a group of periodic slots etched near the front facet to suppress the extra longitudinal modes and achieve a narrow linewidth, and a pair of passive superpartner waveguides located on both sides to filter out the high-order lateral modes in the broad waveguide. The device measured under the temperature of 25 °C shows an output power of 113 mW, a single-lobe lateral far-field distribution with the full width at half maximum of 7.8°, a peak wavelength of 1559.7 nm with the side-mode suppression ratio of 48.5 dB, and an intrinsic linewidth of 230 kHz at the bias current of 800 mA. The device is a promising candidate for cost-effective light sources for coherent communication systems and LiDARs.

Keywords: supersymmetric semiconductor laser; high power; single mode; narrow linewidth

Citation: Xu, Y.; Fu, T.; Fan, J.; Liu, W.; Qu, H.; Wang, M.; Zheng, W. High-Power Supersymmetric Semiconductor Laser with a Narrow Linewidth. *Photonics* **2023**, *10*, 238. https://doi.org10.3390/photonics10030238/

Received: 31 January 2023
Revised: 15 February 2023
Accepted: 21 February 2023
Published: 22 February 2023

1. Introduction

Single-frequency and high-power semiconductor lasers near 1550 nm, with the advantages of eye safety, high coherence and low transmission loss, have a wide range of applications such as free-space optical communications, LiDARs, dense wavelength division multiplexing systems, and photonic integrated circuits [1–4]. These applications require a narrow-linewidth laser source with a high output power under the single-spatial-mode operation. The spectral linewidth, mainly determined by the spontaneous emission entering the lasing mode, is inversely proportional to the photon density in the cavity and therefore decreases with the increase of the output optical power [5], but it is difficult for monolithic semiconductor lasers to obtain the narrow linewidth and the high power simultaneously. The single-mode operation is usually achieved by employing a narrow ridge waveguide to cut off high-order modes in the lateral direction [6]. However, the maximum allowable output power for the narrow-ridge-waveguide laser is limited by the catastrophic optical mirror damage (COMD) or the thermal rollover effect resulting from the small emitting aperture [7]. Although broad stripe lasers can reach very high-power levels, the spectral width tends to be large due to the existence of high-order lasing modes in the cavity.

Various device structures have been reported for high power output while maintaining a single-mode or narrow-linewidth operation at the C-band. By using an asymmetrical cladding composed of the dilute waveguide below the active region of 1 mm long distributed feedback (DFB) semiconductor lasers, a 180 mW output power and a 270 kHz linewidth were demonstrated [8]. The DFB laser based on sampled moiré gratings with a 1 mm cavity length was proposed to reduce the coupling coefficient near the laser facet and the maximum output power of about 183 mW was demonstrated [9]. The 4 mm long slab-coupled optical waveguide DFB laser with the maximum continuous-wave (CW) output power of 850 mW was achieved [10]. The monolithically master oscillator power amplifier (MOPA) with a 2.5 mm total length showed a single-mode output power up to 806 mW under CW conditions [11]. The distributed-Bragg-reflector (DBR) laser integrated with a semiconductor optical amplifier (SOA) achieved a high power of 96 mW and a linewidth of 313 kHz by using the uniform grating in the front mirror and the tapered waveguide in SOA and gain regions [12]. These devices based on the conventional buried grating fabrication technology require regrowth steps to complete the upper epitaxial layers after the gratings are etched, which may affect the reliability and limit the low-cost mass production of devices. To avoid the epitaxial regrowth steps, high-power laterally coupled DFB (LC-DFB) lasers were demonstrated, such as the LC-DFB laser monolithically integrated with a curved tapered SOA (an output power of 210 mW and a linewidth of 64 kHz) [2] and the ridge-waveguide laser with a sidewall first-order diffraction grating (an output power of 150 mW) [13]. The single-mode DFB lasers based on atom-like quantum dot gain material exhibited the output power of 58 mW and the intrinsic linewidth of 30 kHz at 20 °C [14]. However, most reported LC-DFB lasers still rely on the time-consuming and expensive high-precision lithography technologies such as electron beam exposure to define low-order gratings. Single-longitudinal-mode lasers can also be achieved by introducing micron-level slots into one side of the ridge-waveguide as high-order DBR, avoiding the high-resolution lithography and simplifying the fabrication process [15–19]. The slotted laser, composed of a 2 μm wide ridge waveguide integrated with a SOA, achieved output power of >45 mW and spectral linewidth of <500 kHz [16]. The single-mode laser based on the μm-level chirped photonic crystals, with output power of about 33 mW, linewidth of 1 MHz, and modulation bandwidth of 16.63 GHz, was demonstrated [19]. All the reported slotted lasers showed the relatively low output powers (<50 mW) due to the limit of the ridge width (generally $\leq$3 μm to maintain a single-mode operation).

The notion of supersymmetry (SUSY), originating from quantum field theory [20–23], can also be applied to the optical designs because of the similarity between quantum systems and optical systems [24–26]. Many optical devices based on supersymmetry have been reported, such as SUSY mode converters [27] and SUSY lasers [28–32]. The SUSY-based triple-ridge waveguide structure was theoretically designed to achieve a high-power single-lateral mode laser at the wavelength around 1 μm [30]. The single-lobe lateral far-field distribution around 974 nm was demonstrated by the SUSY laser arrays with third-order SUSY transformations near the lasing threshold [32]. However, electrically pumped SUSY semiconductor lasers for the single lateral-mode operation have not been experimentally reported at higher injection current levels. The SUSY lasers near 1550 nm have a great potential to achieve a single lateral mode and simultaneously high output power by the available larger effective index contrast based on AlGaInAs/InP systems compared with those operated at shorter wavelengths [30,32].

In this paper, we have demonstrated a SUSY slotted Fabry–Perot (FP) semiconductor laser near 1550 nm fabricated by the contact-type I-line photolithography. The width of the main waveguide is increased to be 6.5 μm, based on the SUSY design, to obtain a high output power with a single-mode operation. The device measured at the current of 800 mA shows a maximum output power of 113 mW, a single-lobe lateral far-field distribution, a high side-mode suppression ratio (SMSR) of 48.5 dB, and a narrow linewidth of 230 kHz, simultaneously.

2. Design and Fabrication

The schematic of the SUSY slotted FP laser is shown in Figure 1. The main waveguide is formed by an electrically pumped broad ridge waveguide supporting multiple lateral modes. Two passive superpartner waveguides on both sides are designed to couple their modes only with the high-order lateral modes in the main waveguide so as to suppress the lasing of all the undesired modes and thus improve the single-mode output optical power. Additionally, the surface high-order Bragg gratings, composed of periodic slots, are etched near the front facet of the main waveguide to select a single longitudinal mode and achieve a narrow linewidth. The scanning electron microscope (SEM) pictures of the SUSY waveguides and the slots in the fabricated devices are shown in Figure 2a,b, respectively. The AlGaInAs/InP epiwafer used is mainly composed of an n-type InP substrate, an AlGaInAs multiple-quantum-well (MQWs) active layer, a 1.6 μm thick p-type InP cladding layer, and a 0.2 μm thick p-type InGaAs ohmic contact layer. The active layer consists of five compressive-strained wells and six tensile-strained barriers. More details of the epitaxial structure are reported in [33].

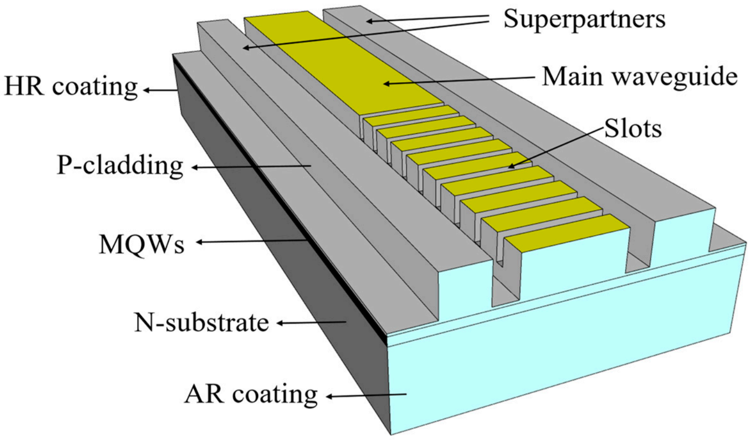

Figure 1. The schematic of the SUSY slotted FP semiconductor laser.

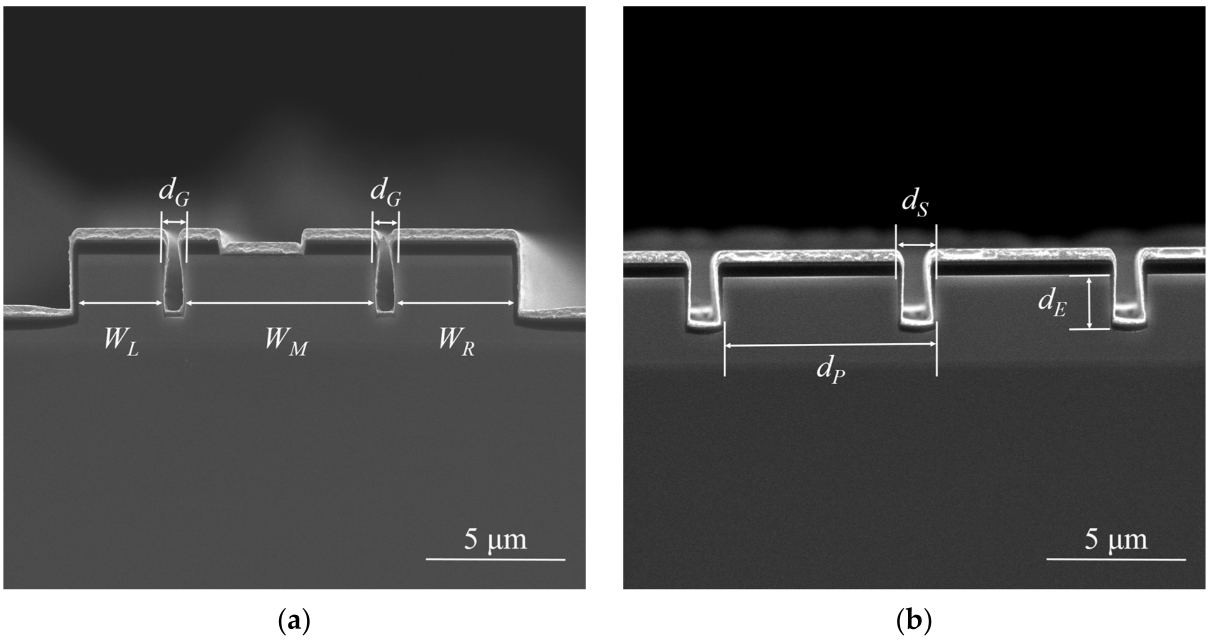

Figure 2. (**a**) The SEM picture of the cross section of the fabricated SUSY waveguides cleaved along the lateral direction. Here, W_L = 2.85 μm, W_M = 6.5 μm, W_R = 4.05 μm, and d_G = 1 μm. (**b**) The SEM picture of the cross-section of the slots cleaved along the longitudinal direction. Here, d_P = 7.5 μm, d_S = 1.1 μm, and d_E = 1.3 μm.

The target wavelength λ is chosen to be 1550 nm in the SUSY structure. The etching depth of all the waveguides is set as 1.75 µm and thus the formed effective refractive index contrast is about 2.6×10^{-2}, which is beneficial to effectively suppress the carrier induced anti-waveguide effect. The trench widths between waveguides are both set as d_G, and the widths of the three waveguides are denoted as W_L (left), W_M (middle), and W_R (right), respectively, as shown in Figure 2a. The maximum W_M for the individual ridge waveguide that can cut off all the high-order lateral modes is only 3 µm at the etching depth of 1.75 µm. A wider main waveguide (W_M = 6.5 µm) is chosen to obtain a higher output power with a single-mode operation by the mode engineering in the designed SUSY structure. The parameter design of the two superpartner waveguides in the following simulation is similar to the method used in [30]. The propagation constant and the corresponding modal loss in the individual waveguide and the SUSY structure are respectively simulated by the commercial software, COMSOL Multiphysics, based on the two-dimensional (2D) finite element method. For the fabricated FP laser based on the epiwafer in [33], the internal loss is ~15 cm^{-1} and the mirror loss with a cavity length of 1 mm and the uncoated facets is ~13 cm^{-1}. In the SUSY structure, only the main waveguide is electrically pumped and thus the materials of the MQWs in the other passive regions of the structure are modeled with complex refractive indices. The corresponding amplitude loss coefficient of the electric field is assumed to be ~14 cm^{-1} in two passive superpartner waveguides. The isolated ridge waveguide (W_M = 6.5 µm) supports three lateral modes, denoted as TE_{M0}, TE_{M1}, and TE_{M2}. The corresponding propagation constants are shown by the black solid lines in Figure 3a.

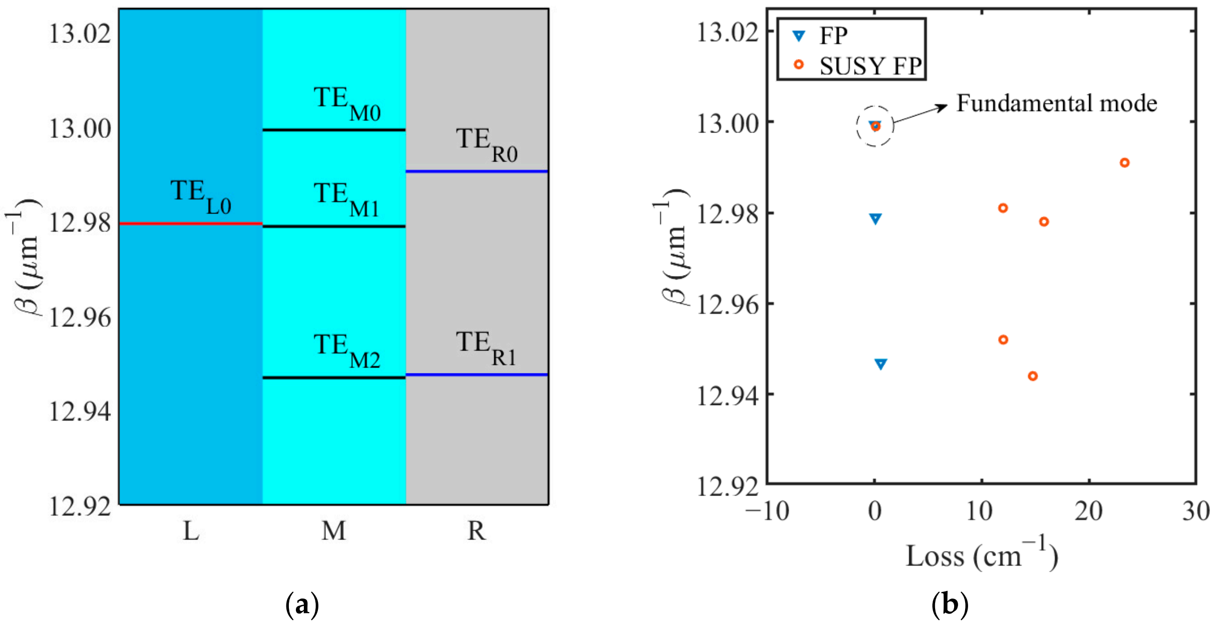

Figure 3. (**a**) Propagation constants of lateral modes in the individual waveguides from the SUSY laser. The red solid line and the blue solid lines are the propagation constants of the left superpartner and the right superpartner, respectively, and the black solid lines represent the propagation constants of the main waveguide. (**b**) The loss of the modes with different propagation constants experienced in the conventional FP and the SUSY FP structure, respectively.

According to the propagation constants of lateral modes versus the width of the individual ridge waveguide, we finally choose W_L to be 2.85 µm and W_R to be 4.05 µm. To meet the pattern resolution demand of the contact-type I-line photolithography and the sufficient mode coupling strength between the main waveguide and the superpartners, the trench width d_G is chosen to be 1 µm. The left superpartner waveguide only supports one mode TE_{L0}, and the right superpartner waveguide supports two modes, TE_{R0} and TE_{R1}, as shown in Figure 3a. Based on the unbroken optical SUSY regime, TE_{L0} of the left superpartner has a counterpart TE_{M1} in the main waveguide, and TE_{R1} of the right superpartner has a counterpart TE_{M2} in the main waveguide. The fundamental mode, without the counterpart in the superpartners, remains almost intact in the main waveguide. In addition, the mode TE_{R0} is hardly coupled with any mode of the main waveguide and mainly confined in the right lossy superpartner. The coupling strength between two modes is determined by the phase detuning and the electric field distributions according to the coupling mode theory. The efficient coupling couples the original modes into a pair of supermodes. As is shown in Figure 3a, we construct lossy superpartners (two passive waveguides in the structure) with propagation constant values that match with those of the modes in the main waveguide except the fundamental mode, and thus all the higher-order modes in the main waveguide split into supermode pairs with larger losses, as shown in Figure 3b. The intensity distributions of the high-order supermodes have a larger spatial overlap with the lossy superpartners. As is shown in Figure 3b, the high-order supermodes suffer larger loss ($\geq$12 cm^{-1}) and thus have higher lasing thresholds than those of the conventional FP (the same width of 6.5 µm) due to the intrinsic loss residing in the passive superpartner waveguides. Therefore, the designed SUSY structure is expected to significantly improve the mode discrimination and achieve a stable single-mode operation in the lateral mode competition.

The slots, shown in Figures 1 and 2b, satisfy Bragg's law and provide enough feedback for the single-longitudinal mode lasing. The slot width d_S and the slot period d_P are expressed as $4n_S d_S = (2m_S + 1)\lambda$ and $2n_{ave}d_P = m\lambda$, respectively, where m_s and m are integers, n_s and n_{ave} are the effective refractive index of the slot region and the average effective refractive index of the whole structure, respectively, and m is the grating order. The slot parameters are optimized based on the 2D scattering matrix method [34] and our previous results [16,30]. We chose d_S to be ~1.1 µm (m_S = 4) for simplifying the fabrication process. There is a trade-off among the maximum reflectivity, the minimum scattering loss caused by the high-order gratings, and the minimum reflection bandwidth [18]. As a result, the slot period d_P is set as 7.5 µm (m = 31), the slot depth d_E is set as 1.3 µm, and the slot number is set as 18.

The fabrication procedures of the SUSY slotted FP laser are similar to those of the conventional ridge-waveguide FP laser. A 300 nm thick SiO_2 layer is firstly deposited by the plasma-enhanced chemical vapor deposition. Then the patterns of micron-level slots are defined by the contact-type I-line photolithography and subsequently transferred to SiO_2 mask layer on the flat wafer surface by the reactive-ion-etching (RIE), which reduces the possibility of the photoresist nonuniformity. By inductively coupled plasma, the slots are etched 1.3 µm deep. After removing the residual SiO_2 mask, the SUSY waveguides are etched 1.75 µm deep by the same process as fabricating the slots. The 300 nm thick SiO_2 insulating layer is deposited on the wafer and then selectively removed to form the electrical injection windows on the surface of the main waveguide by the photolithography and RIE process. Subsequently, p-contact metals are grown by the magnetron sputtering, and then n-contact metals are also deposited after the InP substrate is thinned and polished. Finally, the fabricated wafer is annealed to form ohmic contact and then cleaved into 1 mm long laser bars. The SEM images of the fabricated lasers are shown in Figure 2.

In order to suppress the FP resonance while increasing the output optical power of the SUSY slotted FP laser, the high reflection (HR) coatings to the back facet and anti-reflection (AR, a reflectivity of ~4%) coatings to the front facet are applied. Additionally, the conventional FP laser and the SUSY FP laser (without slots) are also fabricated based on the same epiwafer for the performance analysis. The laser chips are soldered p-side up on the copper heat sinks, the temperature of which is controlled by the thermo electric cooler. All devices are tested under the CW conditions at 25 °C.

3. Results and Discussion

The performances of the three kinds of fabricated semiconductor lasers are characterized. For each laser, the cavity length is 1 mm and the width of the electrically pumped waveguide is 6.5 µm, which is convenient to analyze the effects of the superpartner waveguides or the slots. The power-current curves of the FP laser, the SUSY FP laser, and the SUSY slotted FP laser are separately measured and plotted in Figure 4. For the FP laser, the threshold current is about 40 mA, the slope efficiency is 0.22 mW/mA, and the maximum output power is 161 mW. For the SUSY FP laser, the threshold current is about 65 mA, the slope efficiency is 0.20 mW/mA, and the maximum output power is 147 mW. The trenches (only 1 µm wide) between waveguides are approximately 150 nm shallower than the other regions etched together due to the aspect-ratio dependent etching loading effect. Therefore, the slight performance degradation of SUSY FP laser is mainly attributed to the non-negligible lateral diffusion of the carriers from the main waveguide region. The SUSY slotted FP laser exhibits a threshold current of 75 mA, a slope efficiency of about 0.16 mW/mA, and a maximum output power of 113 mW at a bias current of 800 mA. Compared with the SUSY FP laser without slots, the SUSY slotted FP laser has a higher threshold current and a lower slope efficiency due to the scattering loss caused by the high-order gratings etched near the front facet. In addition, there are some kinks in the power-current curves of the three lasers. The appearance of kinks for the FP laser may be attributed to the high-order modes lasing at higher injection current levels. The high-order modes of the main waveguide possess the same propagation constants as those of the superpartners, but the gain profile between the main waveguide and the superpartners is asymmetric and the supermodes of the SUSY laser experience the spontaneous PT-symmetry breaking as the injection current increases, which leads to the kinks appearing in the power-current curves of two kinds of SUSY lasers [29,35]. The high output power is achieved by increasing the width of the main waveguide to 6.5 µm based on the unbroken SUSY design compared with the conventional slotted FP lasers with a narrow ridge.

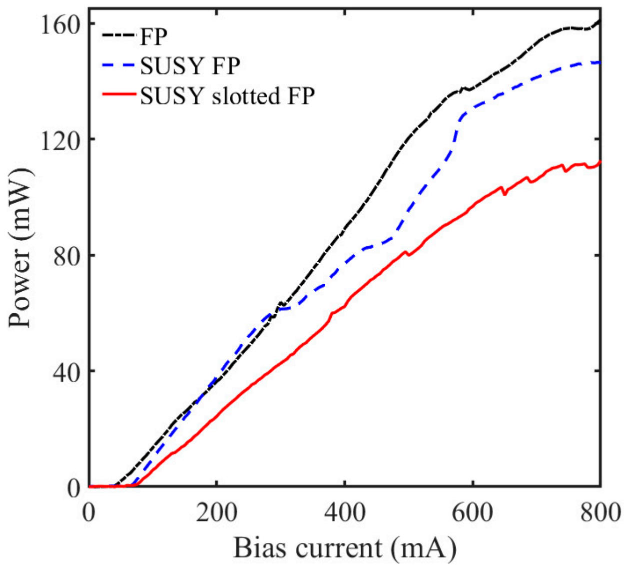

Figure 4. Measured power-current curves of the FP laser, the SUSY FP laser, and the SUSY slotted FP laser.

Figure 5 shows the normalized lateral far-field distributions of the three lasers at an injection current of 800 mA, respectively. For the FP laser, the full width at half maximum (FWHM) of the lateral far-field distribution is the largest (21.0°) because the broad ridge waveguide supports multiple lasing modes and has stronger lateral confinement on the fundamental mode without the coupling effect from the superpartner waveguides. For the SUSY FP laser and the SUSY slotted FP laser, the measured lateral far-field distribution is single-lobe and the corresponding FWHM is 7.6° and 7.8° respectively. The FWHM is nearly three times smaller than that of the FP laser, indicating that only the fundamental supermode can lase in the SUSY structure. In addition, the similar FWHM of the SUSY FP laser and the SUSY slotted FP laser also demonstrates that the introduction of slots has few impacts on the mode filtering of the superpartners. The FWHM of the vertical far-field distribution is ~40° for the three lasers.

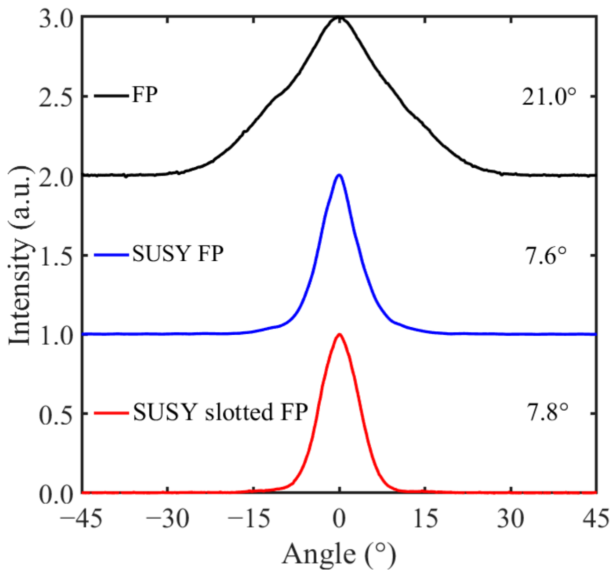

Figure 5. The normalized lateral far-field profiles of the FP laser, the SUSY FP laser, and the SUSY slotted FP laser at a bias current of 800 mA.

The emission optical spectra are measured at 800 mA to characterize different mode behaviors of the FP laser and the SUSY FP laser, as shown in Figure 6. Here, the longitudinal mode spacing of a 1 mm long FP cavity is about 0.36 nm, and thus the high-order lateral modes in each longitudinal-mode peak can be distinguished by the optical spectrum analyzer with a resolution of 0.02 nm. It is obvious that there are three peaks in each longitudinal mode of the FP laser in Figure 6b, which means that the fundamental mode and the two high-order modes are lasing simultaneously. As is shown in Figure 6d, all the longitudinal modes of the SUSY FP laser maintain single-peak lasing, demonstrating that the single-mode operation is achieved, and all the high-order supermodes in the main waveguide are suppressed below the lasing threshold by the loss superpartners. The electrically pumped SUSY semiconductor lasers with a single lateral mode have been firstly realized at the high current level (about ten times of the threshold current). These results are in good agreement with the simulation result of Figure 3a and the lateral far-field distributions in Figure 5.

For the SUSY slotted FP laser, the peak wavelength is 1559.7 nm and the corresponding SMSR is 48.5 dB when the bias current is 800 mA, exhibiting the high spectral purity achieved by the slots, as shown in Figure 7a. The result indicates that the output power of 113 mW is a single-mode optical power in Figure 4, which is much higher than that of the reported narrow-ridge-waveguide slotted FP lasers (<50 mW) [15,16,36]. The lasing wavelength is slightly longer than the designed value (1550 nm), which is mainly attributed to the deviation of the structural parameters caused by the fabrication error and the red-shift of the gain peak at high current levels. The laser linewidth is also measured with the delayed self-heterodyne interferometric technique, as shown in Figure 7b. The output laser is collimated by two collimation lenses (Lens 1 and Lens 2) and a 60-dB isolator focused into a single-mode fiber and then split into two paths by a 1:1 coupler. One path is delayed through a 20 km single-mode fiber and the other path is shifted to 80 MHz by an acousto-optic modulator (AOM) to improve the measurement accuracy. Then, the two paths of light are combined by another 1:1 coupler for beat frequency and converted into the electrical signal through a photodetector (PD). The electrical spectrum analyzer (ESA) is used to measure the radio frequency (RF) spectrum of the beat note signal and then obtain the laser linewidth. Figure 7c shows the RF spectrum of the measured beat note signal at 800 mA. The corresponding fitted Voigt profile gives an FWHM of 1.088 MHz, where the extracted Gaussian FWHM and Lorentzian FWHM are 0.815 MHz and 0.459 MHz, respectively. The Lorentzian part represents the intrinsic noise of the semiconductor laser, and the Gaussian part comes from the technical noise sources such as mechanical vibrations, temperature fluctuations, and injection current noises [37]. The obtained intrinsic linewidth is 230 kHz, equal to half of the Lorentzian part.

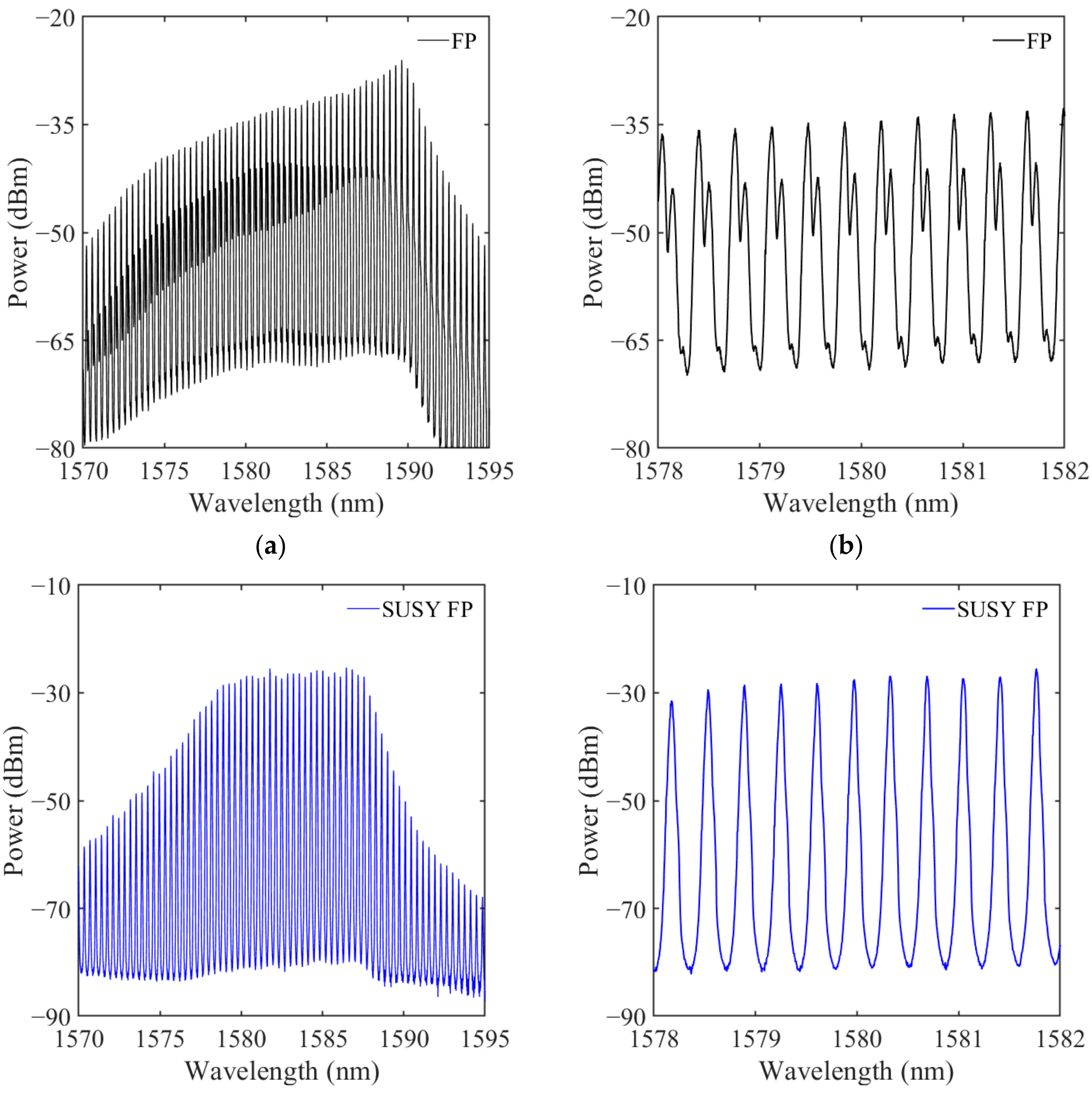

(a) (b) (c) (d)

Figure 6. The optical spectra of (**a**) the FP laser and (**b**) its corresponding enlarged one measured at 800 mA, (**c**) the SUSY FP laser, and (**d**) its corresponding enlarged one measured at 800 mA, respectively.

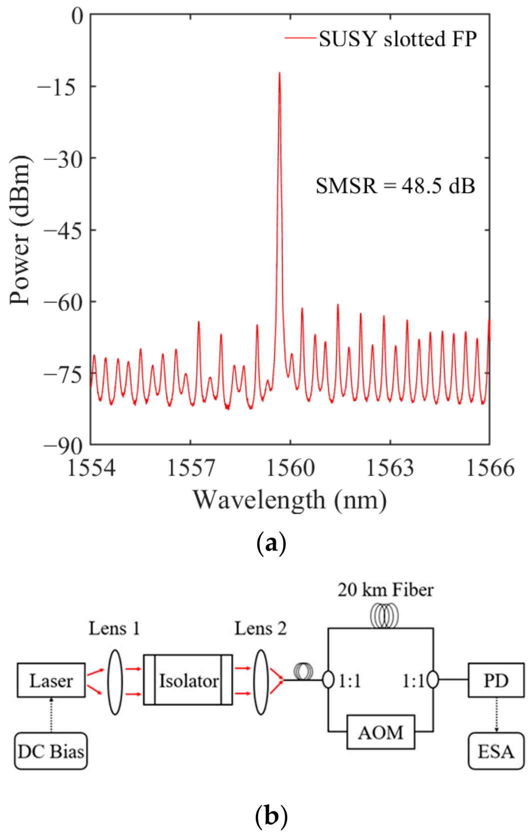

Figure 7. (**a**) Measured output spectrum of the SUSY slotted FP laser at 800 mA. (**b**) Schematic of the delayed self-heterodyne interferometric scheme. (**c**) The normalized RF spectrum of the measured beat note signal and the corresponding Voigt fitting data at 800 mA.

4. Conclusions

In summary, we have demonstrated the SUSY slotted FP semiconductor laser with the characteristics of high output power, single-spatial mode, and narrow linewidth. The device shows an output power of up to 113 mW, a single-lobe lateral far-field pattern with the FWHM of 7.8°, a lasing wavelength of 1559.7 nm with the SMSR of 48.5 dB, and an intrinsic linewidth of 230 kHz at 800 mA. Compared with the previous SUSY laser arrays or slab-coupled optical waveguide lasers, the SUSY structure is simpler in design, compatible with the fabrication of the conventional FP laser, and has no strict requirements for the epitaxial structure, which is promising for low-cost mass production. In future work, we will optimize the dry etching process of InP-based materials, diminish the aspect-ratio dependent etching loading effect, and make the etching depth more uniform in order to achieve a higher-power laser with a lower threshold.

Author Contributions: Conceptualization, W.Z., M.W. and Y.X.; methodology, Y.X. and T.F.; software, Y.X. and T.F.; validation, Y.X. and W.L.; formal analysis, Y.X. and T.F.; investigation, Y.X.; resources, W.Z. and H.Q.; data curation, Y.X. and J.F.; writing—original draft preparation, Y.X.; writing—review and editing, Y.X., T.F. and W.L.; visualization, Y.X. and J.F.; supervision, W.Z. and M.W.; project administration, W.Z. and M.W.; funding acquisition, W.Z., M.W. and H.Q. All authors have read and agreed to the published version of the manuscript.

Funding: This research was funded by the National Key Research and Development Program of China, grant number 2021YFB2801400, and the National Natural Science Foundation of China, grant number 62135001.

Institutional Review Board Statement: Not applicable.

Informed Consent Statement: Not applicable.

Data Availability Statement: Not applicable.

Conflicts of Interest: The authors declare no conflict of interest.

References

1. Selmic, S.; Evans, G.; Chou, T.; Kirk, J.; Walpole, J.; Donnelly, J.; Harris, C.; Missaggia, L. Single frequency 1550-nm AlGaInAs-InP tapered high-power laser with a distributed Bragg reflector. *IEEE Photon. Technol. Lett.* **2002**, *14*, 890–892. [CrossRef]
2. Hou, L.; Haji, M.; Akbar, J.; Marsh, J.H. Narrow linewidth laterally coupled 1.55 μm AlGaInAs/InP distributed feedback lasers integrated with a curved tapered semiconductor optical amplifier. *Opt. Lett.* **2012**, *37*, 4525–4527. [CrossRef]
3. Zhou, P.; Wang, X.; He, Y. A Sub-kHz Narrow-Linewidth, and Hundred-mW High-Output-Power Silicon-Based Er Silicate Laser with Hybrid Pump and Signal Co-Resonant Cavity. *IEEE Photon. J.* **2019**, *12*, 1500212. [CrossRef]
4. Wang, H.; Zhang, R.; Kan, Q.; Lu, D.; Wang, W.; Zhao, L. High-Power Wide-Bandwidth 1.55-μm Directly Modulated DFB Lasers for Free Space Optical Communications. In Proceedings of the Conference on Lasers and Electro-Optics, San Jose, CA, USA, 5–10 May 2019; p. JTu2A.72.
5. Henry, C.H. Theory of the linewidth of semiconductor lasers. *IEEE J. Quantum Electron.* **1982**, *18*, 259–264. [CrossRef]
6. Wenzel, H.; Bugge, F.; Dallmer, M.; Dittmar, F.; Fricke, J.; Hasler, K.; Erbert, G. Fundamental-lateral mode stabilized high-power ridge-waveguide lasers with a low beam divergence. *IEEE Photon. Technol. Lett.* **2008**, *20*, 214–216. [CrossRef]
7. Ziegler, M.; Tomm, J.W.; Zeimer, U.; Elsaesser, T. Imaging Catastrophic Optical Mirror Damage in High-Power Diode Lasers. *J. Electron. Mater.* **2010**, *39*, 709–714. [CrossRef]
8. Faugeron, M.; Michael, T.; Parillaud, O.; Chtioui, M.; Robert, Y.; Vinet, E.; Enard, A.; Jacquet, J.; Van Dijk, F. High-Power Tunable Dilute Mode DFB Laser with Low RIN and Narrow Linewidth. *IEEE Photon. Technol. Lett.* **2013**, *25*, 7–10. [CrossRef]
9. Liu, S.; Wu, H.; Shi, Y.; Qiu, B.; Xiao, R.; Chen, M.; Xue, H.; Hao, L.; Zhao, Y.; Lu, J. High-power single-longitudinal-mode DFB semiconductor laser based on sampled Moiré grating. *IEEE Photon. Technol. Lett.* **2019**, *31*, 751–754. [CrossRef]
10. Mao, Y.; Cheng, Y.; Xu, B.; Ji, R.; Li, Y. Record-High Power 1.55-μm Distributed Feedback Laser Diodes for Optical Communication. In Proceedings of the Optical Fiber Communication Conference (OFC), Washington, DC, USA, 6–11 June 2021; p. W1B.7.
11. Wang, H.; Zhang, R.; Lu, D.; Wang, W.; Zhao, L. Monolithic High Power Master Oscillator Power Amplifier Emitting 2.2 W at 1550 nm. In Proceedings of the 2021 Asia Communications and Photonics Conference (ACP), Shanghai, China, 24–27 October 2021; pp. 1–3.
12. Zhang, G.; Ding, Z.; Wang, K.; Jiang, C.; Lou, J.; Lu, Q.; Guo, W. Demonstration of high output power DBR laser integrated with SOA for the FMCW LiDAR system. *Opt. Exp.* **2022**, *30*, 2599–2609. [CrossRef]
13. Bagaeva, O.G.O.; Galiev, R.R.; Danilov, A.I.; Ivanov, A.V.; Kurnosov, V.D.; Kurnosov, K.V.; Kurnyavko, Y.V.; Ladugin, M.A.E.; Marmalyuk, A.A.E.; Romantsevich, V.I. Experimental studies of 1.5–1.6 μm high-power single-frequency semiconductor lasers. *Quantum Electron.* **2020**, *50*, 143. [CrossRef]
14. Septon, T.; Becker, A.; Gosh, S.; Shtendel, G.; Sichkovskyi, V.; Schnabel, F.; Sengül, A.; Bjelica, M.; Witzigmann, B.; Reithmaier, J.P. Large linewidth reduction in semiconductor lasers based on atom-like gain material. *Optica* **2019**, *6*, 1071–1077. [CrossRef]
15. Lu, Q.; Abdullaev, A.; Nawrocka, M.; Guo, W.-H.; O'Callaghan, J.; Donegan, J.F. Slotted single mode lasers integrated with a semiconductor optical amplifier. *IEEE Photon. Technol. Lett.* **2013**, *25*, 564–567. [CrossRef]
16. Abdullaev, A.; Lu, Q.; Guo, W.; Wallace, M.J.; Nawrocka, M.; Bello, F.; Benson, A.; O'Callaghan, J.; Donegan, J.F. Improved performance of tunable single-mode laser array based on high-order slotted surface grating. *Opt. Exp.* **2015**, *23*, 12072–12078. [CrossRef] [PubMed]
17. Chen, H.; Jia, P.; Chen, C.; Qin, L.; Chen, Y.; Huang, Y.; Ning, Y.; Wang, L. Narrow linewidth DBR laser based on high order Bragg grating defined by i-line lithography. *Opt. Commun.* **2019**, *445*, 296–300. [CrossRef]
18. Du, F.; Xu, Y.; Li, J.; Wang, H.; Zheng, W. Quasi-continuous tunable semiconductor laser based on the gain-lever effect with full C-band coverage fabricated by standard lithography. *Appl. Opt.* **2022**, *61*, 7343–7348. [CrossRef]
19. Li, J.; Wang, X.; Xu, Y.; Du, F.; Wang, M.; Wang, H.; Zheng, W. Single-Mode Laser with Chirped Photonic Crystal Structure Based on Standard Photolithography. *IEEE Photon. Technol. Lett.* **2022**, *34*, 1187–1190. [CrossRef]
20. Neveu, A.; Schwarz, J.H. Factorizable dual model of pions. *Nucl. Phys. B* **1971**, *31*, 86–112. [CrossRef]
21. Ramond, P. Dual theory for free fermions. *Phys. Rev. D* **1971**, *3*, 2415. [CrossRef]
22. Fayet, P.; Ferrara, S. Supersymmetry. *Phys. Rep.* **1977**, *32*, 249–334. [CrossRef]
23. Cooper, F.; Khare, A.; Sukhatme, U. Supersymmetry and quantum mechanics. *Phys. Rep.* **1995**, *251*, 267–385. [CrossRef]
24. Miri, M.-A.; Heinrich, M.; Christodoulides, D.N. Supersymmetry-generated complex optical potentials with real spectra. *Phys. Rev. A* **2013**, *87*, 043819. [CrossRef]
25. Miri, M.-A.; Heinrich, M.; El-Ganainy, R.; Christodoulides, D.N. Supersymmetric optical structures. *Phys. Rev. Lett.* **2013**, *110*, 233902. [CrossRef] [PubMed]
26. Miri, M.-A.; Heinrich, M.; Christodoulides, D.N. SUSY-inspired one-dimensional transformation optics. *Optica* **2014**, *1*, 89–95. [CrossRef]
27. Heinrich, M.; Miri, M.-A.; Stützer, S.; El-Ganainy, R.; Nolte, S.; Szameit, A.; Christodoulides, D.N. Supersymmetric mode converters. *Nat. Commun.* **2014**, *5*, 3698. [CrossRef] [PubMed]

28. Hokmabadi, M.P.; Nye, N.S.; El-Ganainy, R.; Christodoulides, D.N.; Khajavikhan, M. Supersymmetric laser arrays. *Science* **2019**, *363*, 623–626. [CrossRef]
29. Qiao, X.; Midya, B.; Gao, Z.; Zhang, Z.; Zhao, H.; Wu, T.; Yim, J.; Agarwal, R.; Litchinitser, N.M.; Feng, L. Higher-dimensional supersymmetric microlaser arrays. *Science* **2021**, *372*, 403–408. [CrossRef]
30. Zhao, X.; Zeng, S.; Sweatt, L.; Zhu, L. High-power single-mode triple-ridge waveguide semiconductor laser based on supersymmetry. *AIP Adv.* **2021**, *11*, 095216. [CrossRef]
31. Fu, T.; Qi, A.; Chen, J.; Wang, Y.; Zhou, X.; Wang, X.; Dai, Y.; Wang, M.; Zheng, W. Electrically injected supersymmetric semiconductor lasers with narrow vertical divergence angle. *Opt. Lett.* **2022**, *47*, 2991–2994. [CrossRef]
32. Fu, T.; Chen, J.; Wang, Y.; Zhou, X.; Qi, A.; Wang, X.; Dai, Y.; Wang, M.; Zheng, W. Electrically driven supersymmetric semiconductor laser arrays with single-lobe far-field patterns. *Opt. Exp.* **2023**, *31*, 1858–1867. [CrossRef]
33. Wang, M.; Wang, H.; Ma, P.; Dong, F.; Liu, A.; Zheng, W. Eight-channel laser array with 100 GHz channel spacing based on surface-slotted structures fabricated by standard lithography. *Opt. Lett.* **2018**, *43*, 4867–4870. [CrossRef] [PubMed]
34. Lu, Q.; Guo, W.; Phelan, R.; Byrne, D.; Donegan, J.; Lambkin, P.; Corbett, B. Analysis of slot characteristics in slotted single-mode semiconductor lasers using the 2-D scattering matrix method. *IEEE Photon. Technol. Lett.* **2006**, *18*, 2605–2607. [CrossRef]
35. Fu, T.; Wang, Y.; Zhou, X.; Du, F.; Fan, J.; Wang, X.; Chen, J.; Qi, A.; Zheng, W. Approaches to tuning the exceptional point of PT-symmetric double ridge stripe lasers. *Opt. Exp.* **2021**, *29*, 20440–20448. [CrossRef]
36. Wang, Y.; Yang, Y.; Zhang, S.; Wang, L.; He, J.-J. Narrow linewidth single-mode slotted Fabry–Pérot laser using deep etched trenches. *IEEE Photon. Technol. Lett.* **2012**, *24*, 1233–1235. [CrossRef]
37. Spiessberger, S.; Schiemangk, M.; Wicht, A.; Wenzel, H.; Brox, O.; Erbert, G. Narrow linewidth DFB lasers emitting near a wavelength of 1064 nm. *J. Lightw. Technol.* **2010**, *28*, 2611–2616. [CrossRef]